Journal of Materials Chemistry C

Accepted Manuscript

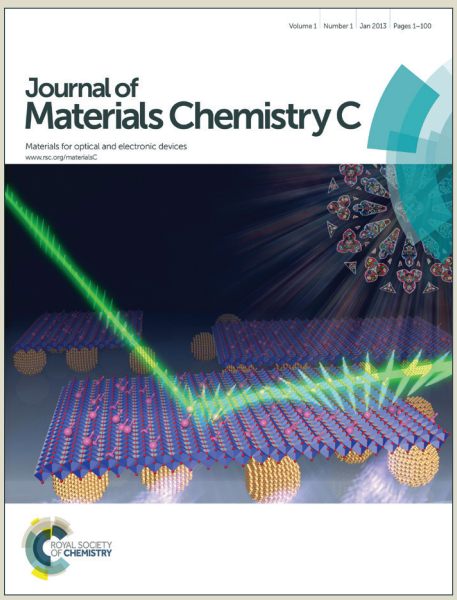

ROYAL SOCIETY OF CHEMISTRY

www.rsc.org/materialsC

Design of liquid crystals with 'de Vries-like' properties: The effect of carbosilane nanosegregation in 5-phenyl-1,3,4-thiadiazole mesogens. ‡

Kirk M. Mulligan,[†] Andreas Bogner,[¶] Qingxiang Song,[†] Christopher P. J. Schubert,[†] Frank Giesselmann[¶] and Robert P. Lemieux*,[†]

[†] *Chemistry Department, Queen's University, Kingston, Ontario, Canada*

[¶] *Institute of Physical Chemistry, University of Stuttgart, Pfaffenwaldring 55, D-70569 Stuttgart, Germany*

Email: lemieux@chem.queensu.ca

‡ Electronic Supplementary Information (ESI) available:

Detailed experimental and synthetic procedures, polarized optical microscopy data.

Table of Content Entry

X-ray diffraction analyses reveal the dependence of 'de Vries-like' properties on the degree of nanosegregation in carbosilane-terminated smectic liquid crystals

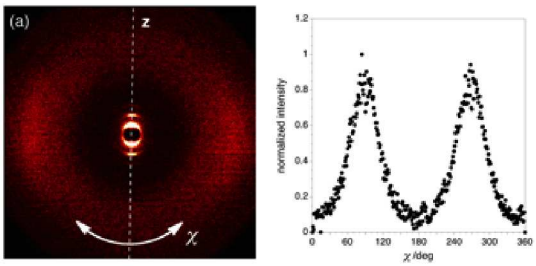

Abstract

Smectic liquid crystals with 'de Vries-like' properties are characterized by a maximum layer contraction of ≤ 1% upon transition from the orthogonal SmA phase to the tilted SmC phase. A defining structural characteristic of most 'de Vries-like' materials is a nanosegregating element that strongly promotes the formation of smectic layers. We show herein the effect of varying the length of a nanosegregating carbosilane end-group on 'de Vries-like' properties in three series of 5-phenyl-1,3,4-thiadiazole mesogens with chloro-terminated alkoxy chains (**QL13-*n*, QL18-*n*** and **QL19-*n***). Shortening the end-group from a tricarbosilane to a monocarbosilane causes a decrease in 'de Vries-like' character, as measured by the reduction factor *R,* which is consistent with a decrease in nanosegregation and quality of the lamellar ordering. Measurements of the orientational order parameter S_2 by 2D X-ray scattering of smectic monodomains show a concomitant increase in S_2 that is consistent with the hypothesis that 'de Vries-like' behavior in these materials arises from a combination of high lamellar order and low orientational order. The requirement of a nanosegregating structural element to achieve 'de Vries-like' behavior is confirmed by the characterization of the chloro-terminated mesogen 2-(6-chlorohexyloxy)-5-(4-hexyloxyphenyl)-1,3,4-thiadiazole (**QL28-6/6**), which undergoes a SmA-SmC transition with a maximum layer contraction of 4.1% and behaves like a conventional smectogen.

Introduction

Liquid crystals with 'de Vries-like' properties form lamellar (smectic) liquid crystal phases and undergo a transition from the orthogonal smectic A (SmA) phase to the tilted smectic C (SmC) phase with a maximum layer contraction of < 1%,[1] as opposed to the layer contraction of 7-10% that occurs with conventional smectic liquid crystals currently used in surface-stabilized ferroelectric liquid crystal (SSFLC) microdisplays.[2-4] Smectic liquid crystals with 'de Vries-like' properties have the potential to solve the intractable problem of chevron formation in SSFLC displays, which results from a buckling of smectic layers on cooling from the SmA to the SmC phase; the formation of chevrons of opposite fold directions produces zigzag line defects that severely degrade the optical quality of SSFLC films.[5] Although zigzag line defects can be avoided by controlling the chevron fold direction with appropriate surface treatment and alignment conditions, the chevron geometry in SSFLC displays invariably results in significantly lower brightness, contrast and viewing angle relative to what could be achieved with a chevron-free bistable bookshelf geometry.[4]

De Vries was the first to explain the unusually small layer contraction of materials known today as 'de Vries-like' liquid crystals using a *diffuse cone* model in which mesogens in the SmA phase have a tilted orientation and a degenerate azimuthal distribution;[6] more recent theoretical work suggests that 'de Vries-like' behavior in mesogens with strong nanosegregrating elements may result from a combination of high lamellar order and low orientational order.[1, 7-10] Chiral 'de Vries-like' liquid crystals tend to have unusually large electroclinic tilt susceptibilities, with the electric field-induced optical tilt accompanied by a large increase in birefringence and minimal contraction of the smectic layer spacing.[1] The electro-optical behavior of two such materials with first-order SmA*-SmC* transitions was recently explained using a generalized Langevin-Debye model, which assumes a random azimuthal distribution of molecules on a fixed tilt cone of angle θ, with an orientational distribution in which the tilt θ is allowed to vary with the applied field over a prescribed range.[11]

A defining structural characteristic of most 'de Vries-like' materials is a nanosegregating element that strongly promotes the formation of smectic layers, such as a trisiloxane end-group or a perfluoroether chain. Trisiloxane end-groups promote the lamellar ordering of calamitic mesogens due to the tendency of trisiloxane and hydrocarbon segments to nanosegregate into distinct sublayers, which results in the formation of partially intercalated smectic bilayers.[12] The amphiphilicity of organosiloxane mesogens is due in part to the relatively shallow torsional potential surfaces of trisiloxane end-groups, which impart a more liquid-like property and approximate spherical shape to these segments relative to the rod-like hydrocarbon segments.[13-15] Organosiloxane mesogens are known to form very stable SmC phases, which may be due to a suppression of out-of-layer fluctuations due to nanosegregation that reduces the entropic cost of molecular tilt. More recently, chemically inert tricarbosilane end-groups have been substituted for the hydrolytically labile trisiloxanes in smectic mesogens that may be more suitable for liquid crystal display applications.[16-18]

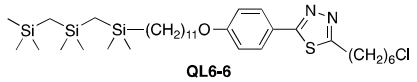

QL6-6

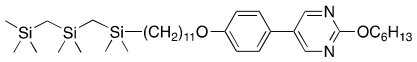

QL16-6

In order to expand a rather limited library of 'de Vries-like' mesogens for the formulation of chevron-free mixtures for bistable SSFLC displays, we developed a molecular design that combines a nanosegregating end-group as SmC-promoting element with a SmA-promoting element such as a chloro-terminated alkyl chain or a 5-phenylpyrimidine core.[17-20] For example, the 5-phenyl-1,3,4-thiadiazole and 5-phenylpyrimidine derivatives **QL6-6** and **QL16-6** undergo a SmA-SmC transition with a maximum layer contraction of only 0.4-0.5%; these materials have reduction factors R at 10 K below the SmA-SmC transition temperature T_{AC} of 0.20 and 0.17, respectively,[17, 18] and rank among the best 'de Vries-like' liquid crystals reported heretofore.[13, 21] The reduction factor R (eqn (1)) is a measure of 'de Vries-like' character defined as the ratio of the tilt angle δ□□□ required to give a layer contraction $d_C(T)/d_{AC}$ at a temperature T below T_{AC}, assuming a conventional model of hard spherocylinders, over the optical tilt angle θ_{opt} measured

by polarized optical microscopy.[22] According to eqn (1), a SmA-SmC transition would approach the limiting case of a perfect 'de Vries' transition as R approaches 0.

$$R = \delta(T)/\theta_{opt}(T) = \cos^{-1}[d_C(T)/d_{AC}]/\theta_{opt}(T) \quad (1)$$

The profiles of relative layer spacing d/d_{AC} *vs.* reduced temperature $T–T_{AC}$ exhibited by these materials, as well as most other 'de Vries-like' materials,[1] show a pronounced negative thermal expansion in the SmA phase that persists on cooling into the SmC phase and counteracts the layer contraction caused by tilting to such an extent that the layer spacing at the SmA-SmC transition is restored, as shown in Fig. 1. Recent analyses by 2D X-ray scattering of smectic monodomains formed by some 'de Vries-like' organosiloxane liquid crystals have shown that the layer contraction due to molecular tilt upon SmA-SmC transition is compensated either by an increase in the orientational order parameter S_2, or by a decrease in interdigitation of the smectic bilayers.[23-25] In the case of the tricarbosilane **QL16-6**, we have recently shown that 'de Vries-like' behavior may be due to the combined effect of an increase in S_2 and a decrease in bilayer interdigitation with decreasing temperature.[18]

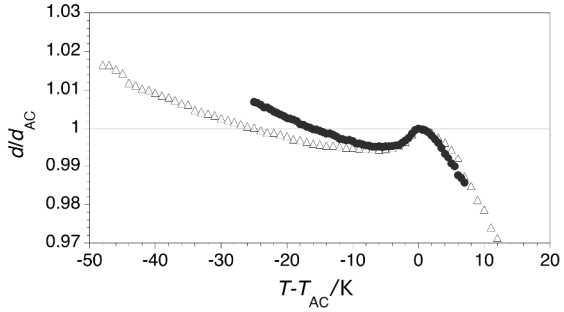

Fig. 1. Relative smectic layer spacing d/d_{AC} *vs*. reduced temperature $T–T_{AC}$ for compounds **QL6-6** (△) and **QL16-6** (●). From refs. 17 and 18.

As part of an ongoing effort to tune 'de Vries-like' properties in carbosilane mesogens,[17, 18] we recently prepared the chloroalkoxy derivative **QL13-6** as an analogue of **QL6-6** based on our observation that the model compound 2-octyloxy-5-(4-octyloxyphenyl)-1,3,4-thiadiazole forms a broader SmC phase than the sterically equivalent analogue 2-nonyl-5-(4-octyloxyphenyl)-1,3,4-thiadiazole.[26] However, we found that **QL13-6** forms *only* a SmC phase (Table 1) despite the

well-documented SmA-promoting effect of the chloro end-group.[27-29] In this paper, we investigate homologous series of the tricarbosilane **QL13-*n***, the dicarbosilane **QL18-*n*** and the monocarbosilane **QL19-*n*** in an effort to produce mesogens with a dialkoxy 5-phenyl-1,3,4-thiadiazole scaffold that form both SmA and SmC phases. We base our approach on empirical knowledge that (i) shorter alkyl chains favor the formation of a SmA phase,[30] and that (ii) shortening the carbosilane end-group should reduce the degree of nanosegregation and therefore favor the formation of a SmA phase.[18] Analyses of these new mesogens by small angle X-ray scattering (SAXS) and 2D X-ray scattering of smectic monodomains reveal that 'de Vries-like' behavior depends on the degree of nanosegregation imposed by the carbosilane end-group, and that the latter is essential for any 'de Vries-like' behavior to be observed in these materials.

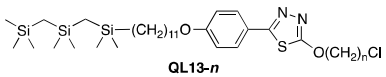

QL13-*n*

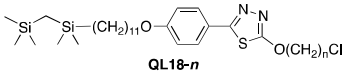

QL18-*n*

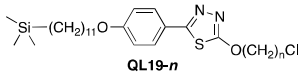

QL19-*n*

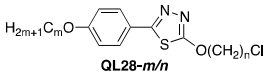

QL28-*m/n*

Results and discussion

Synthesis and characterization

The carbosilane mesogens **QL13-*n***, **QL18-*n*** and **QL19-*n*** were derived from 2,5-dibromo-1,3,4-thiadiazole[31] using a modification of the synthesis of 2-alkoxy-5-(4-cyanophenyl)-1,3-thiazole by Grubb *et al.*, as shown in Scheme 1 (see ESI for details).[32, 33] The non-carbosilane derivatives **QL28-*m/n*** were prepared following a similar route using 1-alkoxy-4-bromobenzene precursors instead of the carbosilane-terminated precursors **3**-**5**. The mesophases formed by these new compounds (Table 1) were characterized by polarized optical microscopy (POM) and differential scanning calorimetry (DSC).

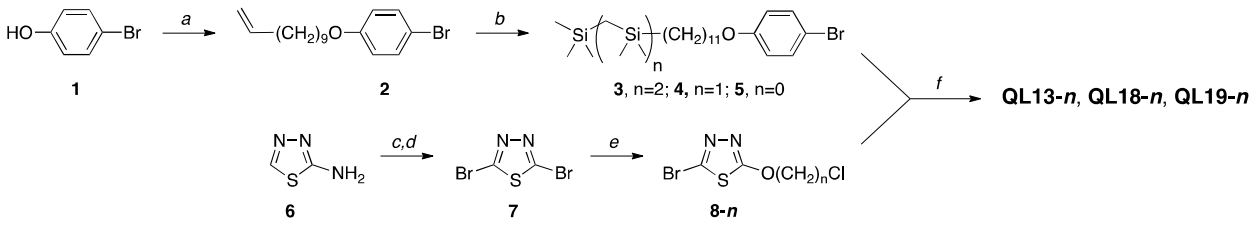

Scheme 1. *Reagents and conditions*: (a) CH_2=$CH(CH_2)_9OH$, DIAD, Ph_3P, THF; (b) 2,2,4,4,6-pentamethyl-2,4,6-trisilaheptane or 2,2,4-trimethyl-2,4-disilapentane, Karsted's catalyst, toluene (for n=2 and n=1, respectively); or (i) chlorodimethylsilane, Karsted's catalyst, toluene, then (ii) CH_3MgBr (for n=0); (c) Br_2, NaOAc, AcOH; (d) HBr, $NaNO_2$, CuBr; (e) $Cl(CH_2)_nOH$, NaH, CuO, KI, THF; (f) *n*-BuLi, $ZnCl_2$(TMEDA), $Pd(PPh_3)_4$, THF.

Table 1. Transition temperatures (°C) and enthalpies of transitions (kJ mol^{-1}, in parentheses) for compounds **QL13-*n*, QL17-*n*, QL18-*n*** and **QL28-*m*/*n***.[a]

Compound	Cr	Cr'	SmB	SmC	SmA	I
QL13-3	• 17 (28)			• 62 (< 0.1)[b]	• 66 (7.7)	•
QL13-4	• –2 (7.9)	• 5 (2.5)		•	72 (9.2)	•
QL13-5	• 32	• 36 (23)[c]		•	75 (10)	•
QL13-6	• 24 (18)			•	78 (13)	•
QL18-3	• 26 (20)			• 66 (< 0.1)[b]	• 77 (8.8)	•
QL18-4	• 13 (10)			• 76 (< 0.1)[b]	• 80 (9.1)	•
QL18-5	• 40	• 44 (25)[c]		• 82 (< 0.1)[b]	• 84 (11)	•
QL18-6	• 33	• 36 (22)[c]		•	83 (13)	•
QL19-3	• 56 (38)				• 87 (4.4)	•
QL19-4	• 33 (17)				• 88 (8.8)	•
QL19-5	• 45 (25)				• 91 (11)	•
QL19-6	• 36 (19)			• 63 (< 0.1)[b]	• 90 (10)	•
QL28-6/6	• 55 (20)			• 58 (< 0.1)[b]	• 81 (6.1)	•
QL28-11/6	• 63 (40)		(• 52 (1.5))[d]		• 92 (11)	•

[a] Measured by DSC on heating, unless otherwise noted. [b] Transition temperature measured by polarized microscopy. [c] Total enthalpy for both transitions due to partial resolution of the peaks. [d] Monotropic mesophase measured by DSC on cooling.

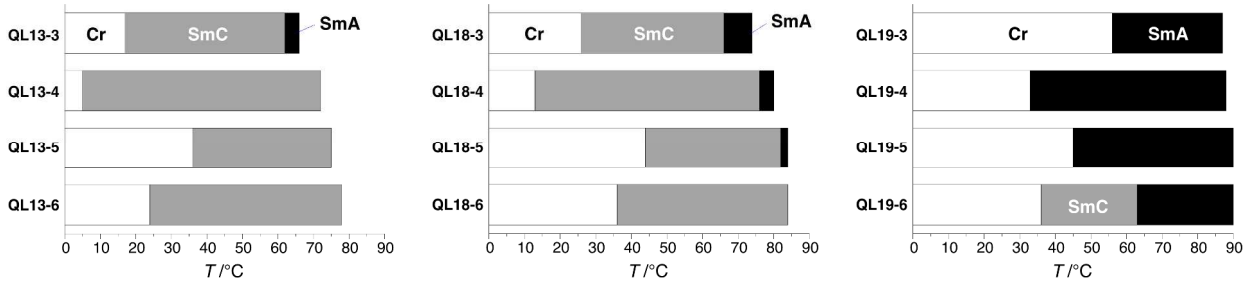

Fig. 2. Mesophases formed on heating by compounds **QL13-*n***, **QL18-*n*** and **QL19-*n***.

As shown graphically in Fig. 2, all carbosilane mesogens form enantiotropic SmA and/or SmC phases. The orthogonal SmA phase was characterized by the formation of fan textures and homeotropic domains under POM, which turned into broken fan and Schlieren textures upon transition to the tilted SmC phase (see ESI). Texture analysis of unaligned 10 μm films revealed

a significant change in interference color on cooling **QL13-3** and (to a lesser extent) **QL18-3** from the SmA to the SmC phase, which is consistent with similar changes observed with 'de Vries-like' liquid crystals, and is indicative of an increase in orientational order (see ESI).[1, 17, 18, 20] By contrast, neither **QL19-6** nor the non-carbosilane **QL28-6/6** showed any significant change in interference color on cooling from the SmA to the SmC phase. The monotropic SmB phase formed by **QL28-11/6** was detected by DSC on cooling and characterized by a sharpening of the fan texture upon transition from the SmA phase.[34]

In order to produce a SmA-SmC phase sequence in the tricarbosilane series **QL13-*n***, the chloroalkoxy chain had to be shortened to $n = 3$. Substituting the tricarbosilane end-group with a dicarbosilane in series **QL18-*n*** resulted in an incremental change in mesogenic properties: the homologues $n = 3$-5 exhibit a SmA-SmC phase sequence, and the SmA temperature range is inversely proportional to the chain length, as expected from empirical trends. A more profound change in mesogenic properties was observed on further shortening the carbosilane end-group in series **QL19-*n***: the homologues $n = 3$-5 form only SmA phases, and only the longer homologue $n = 6$ exhibits the desired SmA-SmC phase sequence. Overall, shortening the carbosilane end-group resulted in increased melting points (i.e., transition temperatures from the crystalline phase to either the SmA or SmC phase) and clearing points, which is consistent with a previous report on organosiloxane mesogens by Naciri *et al.*[12d] Removing the carbosilane end-group from **QL19-6** to give **QL28-11/6** caused the SmC phase to vanish, and resulted in the formation of a monotropic SmB phase together with the enantiotropic SmA phase. Varying the chain length combination in this scaffold by trial and error led to the homologue **QL28-6/6**, which forms a broad SmA phase and a narrow SmC phase on heating, although the temperature range of the SmC phase extends to ca. 30 K on cooling. To the best of our knowledge, **QL28-6/6** is the first example of a calamitic mesogen without a nanosegregating element in which the presence of a chloro end-group does not completely suppress the SmC phase.[27-29]

Optical tilt angles (θ_{opt}) were measured by POM as a function of reduced temperature $T–T_{AC}$ in the absence of an electric field for those materials that form both SmA and SmC phases.[35] A comparison of $\theta_{opt}(T)$ profiles for two homologous pairs (Fig. 3) shows the effect of shortening the carbosilane end-group on the optical tilt angle, from tricarbosilane to dicarbosilane (**QL13-3** *vs.* **QL18-3**) and from tricarbosilane to monocarbosilane (**QL6-6** *vs.* **QL19-6**). The decrease in θ_{opt} with decreasing length of the carbosilane end-group for a given chloroalkyl chain length is consistent with a weakening of the nanosegregation imposed by the carbosilane end-group and its concomitant SmC-promoting effect.[18]

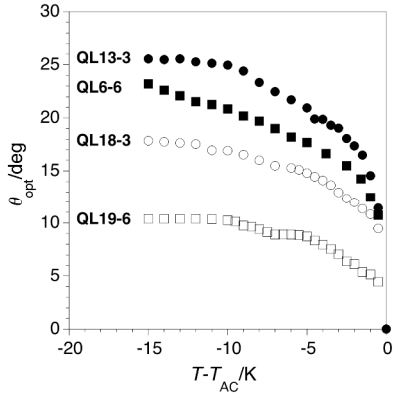

Fig. 3. Optical tilt angle θ_{opt} *vs*. reduced temperature $T–T_{AC}$ measured on cooling for **QL13-3** (●), **QL18-3** (○), **QL6-6** (■) and **QL19-6** (□). The data for **QL6-6** is from ref. 17.

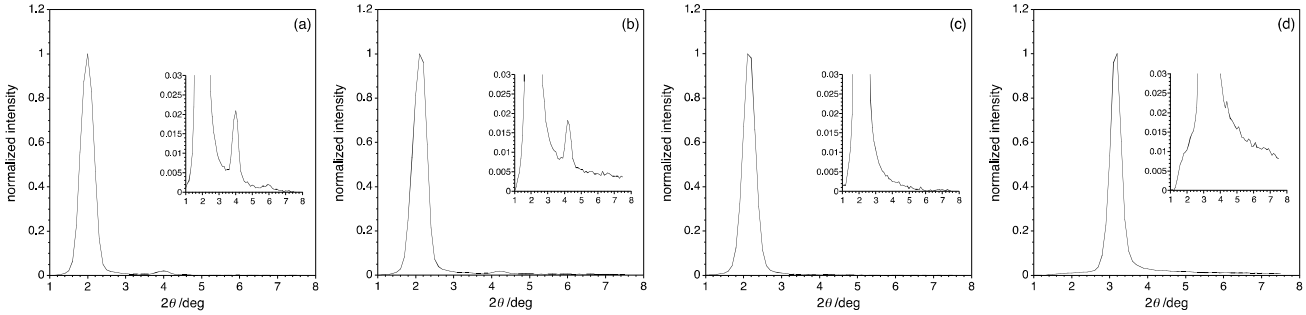

Fig. 4. Normalized intensity profiles of the small angle X-ray scattering produced by (a) **QL13-3**, (b) **QL18-3**, (c) **QL19-6** and (d) **QL28-6/6**.

Small angle X-ray scattering

Accurate measurements of the smectic layer spacing *d* as a function of temperature were carried out by small angle X-ray scattering (SAXS) for the carbosilane mesogens **QL13-3**,

QL18-3 and **QL19-6**, and the non-carbosilane mesogen **QL28-6/6**. The measurements were performed on heating from the crystalline phase except for **QL28-6/6**, which was analyzed on cooling from the isotropic phase. As shown in Fig. 4, the small angle scattering produced by the tricarbosilane **QL13-3** consists of a sharp fundamental and two higher-order quasi-Bragg peaks, which is indicative of a high lamellar order. The scattering intensity profile of **QL18-3** shows only one higher-order peak and those of **QL19-6** and **QL28-6/6** show none, which is consistent with the trend observed with the θ_{opt} measurements and further supports the notion that shortening the carbosilane end-group reduces the lamellar order of these smectogens.

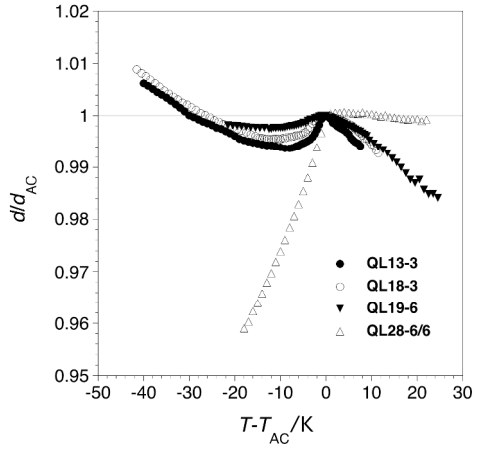

Fig. 5. Relative smectic layer spacing d/d_{AC} *vs*. reduced temperature $T–T_{AC}$ for **QL13-3** (●), **QL18-3** (○), **QL19-6** (▾) and **QL28-6/6** (△). The data for **QL28-6/6** were acquired on cooling from the isotropic liquid phase.

Table 2. Layer spacing d_{AC} and orientational order parameter S_2 measured at T_{AC}, effective molecular length L_{eff} at T_{AC}, calculated molecular length L_{calc}, maximum layer contraction $\%lc_{max}$, optical tilt angle θ_{opt} and reduction factor R at $T–T_{AC} = –10$ K for selected compounds.

Compound	d_{AC}/Å	S_2	L_{eff}/Å	L_{calc}/Å[a]	$\%lc_{max}$	θ□□□/°	R
QL13-3	42.8	0.47	52.0	38.9	0.6	25	0.25
QL18-3	40.2	0.51	48.0	35.8	0.4	17	0.32
QL19-6	39.7	0.57	46.3	37.0	0.2	10	0.39
QL28-6/6	27.4	0.60	31.6	27.7	4.1	13	1.0

[a] Measured from molecular models and include van der Waals radii (B3LYP/6-31G*)

As shown in Fig. 5, the profiles of relative layer spacing d/d_{AC} *vs.* reduced temperature $T–T_{AC}$ for the three carbosilane mesogens show the characteristics of 'de Vries-like' materials, *i.e.*, a negative thermal expansion in the SmA phase that persists in the SmC phase and compensates

for the layer contraction due to molecular tilt; the maximum layer contraction $\%lc_{max}$ ranges from 0.2 to 0.6% (Table 2). The reduction factor R at $T–T_{AC} = –10$ K (eqn 1) increases with decreasing length of the carbosilane end-group—from 0.25 for the tricarbosilane **QL13-3** to 0.39 for the monocarbosilane **QL19-6**—which reflects the concomitant decrease in optical tilt angle θ_{opt}. On the other hand, the profile of the non-carbosilane **QL28-6/6** is characteristic of a conventional model of hard spherocylinders: in the SmA phase, d/d_{AC} is relatively invariant of temperature, and the layer contraction upon the SmA-SmC transition increases with decreasing temperature, reaching a maximum of 4.1% prior to crystallization at $T–T_{AC} = –13$ K.[1]

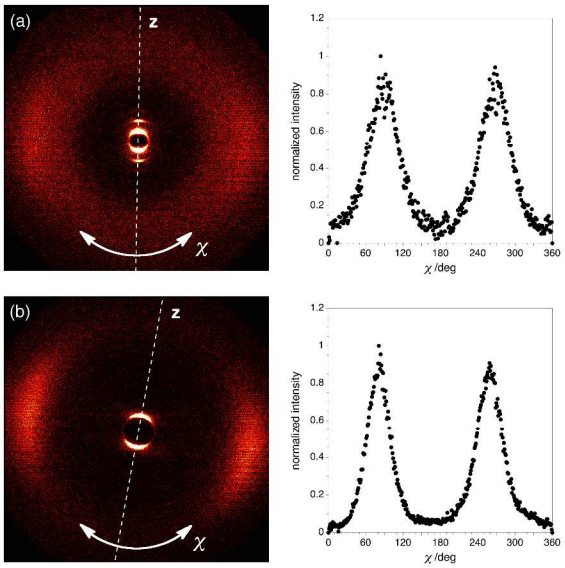

Fig. 6. 2D X-ray scattering patterns from monodomains formed in the SmA phase at $T–T_{AC} = +4$ K (left) and the intensity profiles of the diffuse wide-angle scattering as a function of the azimuthal angle χ (right) for (a) **QL13-3** and (b) **QL28-6/6**. In each case, the normalized intensity *vs.* χ corresponds to the integrated intensity over the wide-angle scattering range of q, which includes both carbosilane and hydrocarbon scattering in the case of **QL13-3**.

Monodomain 2D X-ray scattering

In order to understand the difference in 'de Vries-like' properties between the three types of carbosilane mesogens, we carried out X-ray scattering analyses of smectic monodomains formed by **QL13-3**, **QL18-3**, **QL-19-6** and the non-carbosilane mesogen **QL28-6/6** and measured their orientational order parameters S_2 as a function of temperature.[23, 24] The orientational order parameter is a measure of the orientational order about the director **n** (average direction of all

molecular axes) according to eqn (2), where β is the angle formed by the long axis of a single molecule and **n**. The 2D X-ray scattering patterns of **QL13-3** and **QL28-6/6** at $T–T_{AC}$ = +4 K are shown in Fig. 6 as representative examples. Each pattern features sharp small-angle scatterings along the layer normal **z** corresponding to the layer periodicity and diffuse wide-angle scatterings along an axis orthogonal to **z**, with maxima along the X-ray scattering vector q corresponding to the mean intermolecular distance of the fluid intra-layer correlations. In the case of the tricarbosilane **QL13-3**, one can distinguish an inner wide-angle scattering corresponding to the carbosilane end-groups and a more intense outer wide-angle scattering corresponding to the hydrocarbon segments, which is consistent with the nanosegregation of the two segments. To calculate S_2, wide-angle intensity profiles $I(\chi)$ were obtained by integrating the intensity I scattered along the azimuthal angle χ over the range of q, which includes both the inner carbosilane and outer hydrocarbon scatterings in the case of the three carbosilane mesogens;[18] values of S_2 were obtained by analyzing the $I(\chi)$ profiles according to the method of Davidson *et al*.[36, 37]

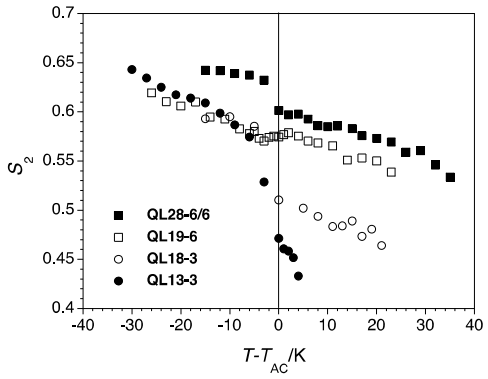

Fig. 7. Orientational order parameter S_2 *vs.* reduced temperature $T–T_{AC}$ for **QL13-3** (●), **QL18-3** (○), **QL19-6** (□) and **QL28-6/6** (■).

As shown in Fig. 7, the $S_2(T)$ profile of the tricarbosilane **QL13-3** is consistent with those of other de 'Vries-like' mesogens with chloro-terminated chains.[23, 25] It shows an increase in S_2 on cooling in the SmA phase—starting from an unusually low value of 0.43—that persists in the SmC phase and reaches a high value of 0.65 prior to crystallization. The $S_2(T)$ profiles of **QL18-3** and **QL19-6** on cooling in the SmA phase also show an increase in S_2—albeit less pronounced

than that of **QL13-3**. However, the three carbosilane mesogens are strikingly different in terms of the magnitude of S_2 in the SmA phase; this difference in orientational order vanishes on cooling into the SmC phase as the profiles of the three carbosilane mesogens appear to merge at ca. $T–T_{AC} = –5$ K.[38] The $S_2(T)$ profile of the non-carbosilane **QL28-6/6** is similar to that of **QL19-6** in the SmA phase except that S_2 values are slightly higher; upon SmA-SmC transition however, the value of S_2 jumps and remains relatively invariant of temperature in the SmC phase, leveling off at the same high value of 0.65 as that of **QL13-3** prior to crystallization.

$$S_2 = 0.5 \langle 3 \cos^2 \beta - 1 \rangle \quad (2)$$

$$L_{eff}(T) = 3d(T)/(S_2(T) + 2) \quad (3)$$

The effective molecular length L_{eff} at T_{AC} is derived from the corresponding values of S_2 and smectic layer spacing d_{AC} according to eqn (3) and may be interpreted as the layer spacing at the SmA-SmC transition *if* the mesogens had a perfect orientational order. As shown in Table 2, L_{eff} values for **QL13-3** and **QL18-3** exceed the calculated lengths L_{calc} of fully extended molecular models minimized at the B3LYP/6-31G* level by a factor of ca. 1.3, which is consistent with an intercalated bilayer structure.[18] This difference in length is somewhat less in the case of the monocarbosilane **QL19-6** but still consistent with an intercalated bilayer structure. The smaller, yet significant difference between L_{eff} and L_{calc} for the non-carbosilane **QL28-6/6** is consistent with those deduced for conventional dialkoxy 2-phenylpyrimidines smectogens,[39] and may be attributed to out-of-layer fluctuations in a smectic monolayer structure.

Conclusions

The results described herein suggest that high lamellar ordering, as produced in this case by the nanosegregation of carbosilane end-groups, is required to achieve 'de Vries-like' behavior. This is shown by the effect of shortening the carbosilane end-group on the reduction factor R, although the most striking effect is that of removing the carbosilane end-group, both on R and on the $d/d_{AC}(T)$ profile. Indeed, the effect on R notwithstanding, it is important to note that all three

carbosilane homologues show similar $d/d_{AC}(T)$ profiles that are characteristic of 'de Vries-like' behavior, i.e., pronounced negative thermal expansion in the SmA phase that persists in the SmC phase and counteracts the layer contraction due to molecular tilt. The difference in R in the three carbosilane series is due to a decrease in θ_{opt} with decreasing length of the carbosilane end-group, which is related to a concomitant decrease in lamellar order. Without a carbosilane end-group—as shown by **QL28-6/6**, the first example of a chloro-terminated mesogen with a SmA-SmC phase sequence that lacks a strong nanosegregating element—the $d/d_{AC}(T)$ profile loses all 'de Vries-like' characteristics. This result dispels the notion that 'de Vries-like' behavior is caused by a 'frustration' between a SmC-promoting element (the dialkoxy 5-phenyl-1,3,4-thiadiazole scaffold in the case of **QL28-6/6**) and a SmA-promoting element (the chloro-terminated chain), as articulated in our original design strategy.[19]

The results show that the other requirement for 'de Vries-like' behavior, a low orientational order, is also affected by the length of the carbosilane end-group, i.e., it is inversely proportional to the length of the latter. The reason why is less evident, and we will need to better understand the structure of the carbosilane sub-layer in order to elucidate this structure-property relationship. Nevertheless, if one assumes that a tricarbosilane is approximately spherical in shape by virtue of shallow torsional potential surfaces, the cross-section of the end-group should decrease with the length of the carbosilane. It is therefore plausible that the nanosegregation of bulky tricarbosilane end-groups in the intercalated bilayer formed by **QL13-3** might create significant free volume in the mesogenic sub-layer, which would be 'filled' by an increase in orientational fluctuations, i.e., a decrease in S_2, in order to minimize free energy. The need for such orientational fluctuations would be reduced in the case of less bulky di- and monocarbosilane end-groups. If this proves to be correct, the tricarbosilane would therefore play a dual role of increasing lamellar order and decreasing orientational order in the intercalated bilayers formed by smectogens such as **QL13-3** in promoting 'de Vries-like' behavior. We are currently carrying out a detailed modeling study

of the bilayer structure formed by these and other carbosilane-terminated mesogens and will report the results of this study in due course.

Acknowledgments

We thank the Natural Sciences and Engineering Research Council of Canada (Discovery and CREATE grants) and the Deutsche Forchungsgemeinschaft (NSF/DFG *Materials World Network* program DFG Gi 243/6) for support of this work.

References

1. J. P. F. Lagerwall and F. Giesselmann, *ChemPhysChem.*, 2006, **7**, 20-45.
2. N. A. Clark and S. T. Lagerwall, *Appl. Phys. Lett.*, 1980, **36**, 899-901.
3. J. W. Goodby, R. Blinc, N. A. Clark, S. T. Lagerwall, M. A. Osipov, S. A. Pikin, T. Sakurai, K. Yoshino and B. Zeks, eds., *Ferroelectric Liquid Crystals: Principles, Properties and Applications*, Gordon & Breach, Philadelphia, 1991.
4. S. T. Lagerwall, *Ferroelectric and Antiferroelectric Liquid Crystals*, Wiley-VCH, Weinheim, 1999.
5. T. P. Rieker, N. A. Clark, G. S. Smith, D. S. Parmar, E. B. Sirota and C. R. Safinya, *Phys. Rev. Lett.*, 1987, **59**, 2658-2661.
6. A. de Vries, *J. Chem. Phys.*, 1979, **71**, 25-31.
7. M. V. Gorkunov, M. A. Osipov, J. P. F. Lagerwall and F. Giesselmann, *Phys. Rev. E*, 2007, **76**, 051706.
8. K. Saunders, D. Hernandez, S. Pearson and J. Toner, *Phys. Rev. Lett.*, 2007, **98**, 197801.
9. S. T. Lagerwall, P. Rudquist and F. Giesselmann, *Mol. Cryst. Liq. Cryst.*, 2009, **510**, 148-157.
10. M. V. Gorkunov, M. A. Osipov, N. Kapernaum, D. Nonnenmacher and F. Giesselmann, *Phys. Rev. E*, 2011, **84**, 051704.

11. Y. Shen, L. Wang, R. Shao, T. Gong, C. Zhu, H. Yang, J. E. Maclennan, D. M. Walba and N. A. Clark, *Phys. Rev. E*, 2013, **88**, 062504.
12. (a) H. J. Coles, H. Owen, J. Newton and P. Hodge, *Liq. Cryst.*, 1993, **15**, 739-744; (b) K. Sunohara, K. Takatoh and M. Sakamoto, *Liq. Cryst.*, 1993, **13**, 283-294; (c) H. Poths, E. Wischerhoff, R. Zentel, A. Schönfeld, G. Henn and F. Kremer, *Liq. Cryst.*, 1995, **18**, 811-818; (d) J. Naciri, J. Ruth, G. Crawford, R. Shashidhar and B. R. Ratna, *Chem. Mater.*, 1995, **7**, 1397-1402; (e) J. Z. Vlahakis, K. E. Maly and R. P. Lemieux, *J. Mater. Chem.*, 2001, **11**, 2459-2464.
13. M. S. Spector, P. A. Heiney, J. Naciri, B. T. Weslowski, D. B. Holt and R. Shashidhar, *Phys. Rev. E*, 2000, **61**, 1579-1584.
14. S. Grigoras and T. H. Lane, *J. Comput. Chem.*, 1988, **9**, 25-39.
15. S. Grigoras and T. H. Lane, *J. Comput. Chem.*, 1987, **8**, 84-93.
16. R. A. Reddy, C. Zhu, R. Shao, E. Korblova, T. Gong, Y. Shen, E. Garcia, M. A. Glaser, J. E. Maclennan, D. M. Walba and N. A. Clark, *Science*, 2011, **332**, 72-77.
17. Q. Song, D. Nonnenmacher, F. Giesselmann and R. P. Lemieux, *J. Mater. Chem. C*, 2013, **1**, 343-350.
18. C. P. J. Schubert, A. Bogner, J. H. Porada, K. Ayub, T. Andrea, F. Giesselmann and R. P. Lemieux, *J. Mater. Chem.*, 2014, **2**, 4581-4589.
19. L. Li, C. D. Jones, J. Magolan and R. P. Lemieux, *J. Mater. Chem.*, 2007, **17**, 2313-2318.
20. J. C. Roberts, N. Kapernaum, Q. Song, D. Nonnenmacher, K. Ayub, F. Giesselmann and R. P. Lemieux, *J. Am. Chem. Soc*, 2010, **132**, 364-370.
21. M. D. Radcliffe, M. L. Brostrom, K. A. Epstein, A. G. Rappaport, B. N. Thomas, R. Shao and N. A. Clark, *Liq. Cryst.*, 1999, **26**, 789-794.
22. Y. Takanishi, Y. Ouchi, H. Takezoe, A. Fukuda, A. Mochizuki and M. Nakatsuka, *Jpn. J. Appl. Phys.*, 1990, **2**, L984-L986.
23. D. Nonnenmacher, S. Jagiella, Q. Song, R. P. Lemieux and F. Giesselmann, *ChemPhysChem.*, 2013, **14**, 2990-2995.

24. H. Yoon, D. M. Agra-Kooijman, K. Ayub, R. P. Lemieux and S. Kumar, *Phys. Rev. Lett.*, 2011, **106**, 087801.

25. D. M. Agra-Kooijman, H. Yoon, S. Dey and S. Kumar, *Phys. Rev. E*, 2014, **89**, 032506.

26. Q. Song, A. Bogner, F. Giesselmann and R. P. Lemieux, *Chem. Commun.*, 2013, **49**, 8202-8204.

27. J. W. Goodby, I. M. Saez, S. J. Cowling, V. Görtz, M. Draper, A. W. Hall, S. Sia, G. Cosquer, S.-E. Lee and E. P. Raynes, *Angew. Chem. Int. Ed.*, 2008, **47**, 2754-2787.

28. I. Rupar, K. M. Mulligan, J. C. Roberts, D. Nonnenmacher, F. Giesselmann and R. P. Lemieux, *J. Mater. Chem. C*, 2013, **1**, 3729-3735.

29. G. F. Starkulla, E. Kapatsina, A. Baro, F. Giesselmann, S. Tussetschläger, M. Kaller and S. Laschat, *Beil. J. Org. Chem.*, 2009, **5**, no. 63.

30. C. S. Hartley, N. Kapernaum, J. C. Roberts, F. Giesselmann and R. P. Lemieux, *J. Mater. Chem.*, 2006, **16**, 2329-2337.

31. D. Xiao, A. Palani, M. Sofolarides, Y. Huang, R. Aslanian, H. Vaccaro, L. Hong, B. McKittrick, R. E. West Jr., S. M. Williams, R.-L. Wu, J. Hwa, C. Sondey and J. Lachowicz, *Bioorg. Med. Chem. Lett.*, 2011, **21**, 861-864.

32. A. M. Grubb, C. Zhang, A. Jakli, P. Sampson and A. J. Seed, *Liq. Cryst.*, 2012, **39**, 1175-1195.

33. Z. M. Hudson, X.-Y. Liu and S. Wang, *Org. Lett.*, 2011, **13**, 300-303.

34. I. Dierking, *Textures of Liquid Crystals*, Wiley-VCH, Weinheim, 2003.

35. The advantages of this method over measuring θ_{opt} by electro-optical switching in the SmC* phase are that (i) no doping with a chiral additive is required, and (ii) there are no possible contribution from an electroclinic effect near T_{AC}. P. Rudquist, private communication.

36. P. Davidson, D. Petermann and A.-M. Levelut, *J. Phys. II France*, 1995, **5**, 113-131.

37. F. Giesselmann, R. Germer and A. Saipa, *J. Chem. Phys.*, 2005, **123**, 034906.

38. Experimental error for S_2 values is ± 0.02.

39. N. Kapernaum, C. S. Hartley, J. C. Roberts, F. Schoerg, D. Krueerke, R. P. Lemieux and F. Giesselmann, *ChemPhysChem.*, 2010, **11**, 2099-2107.